Solvothermal recrystallization of α-calcium sulfate hemihydrate: Batch reactor experiments and kinetic modelling

Nayane Macedo Portela da Silva, Yi Rong, Fabienne Espitalier, Fabien Baillon, Alain Gaunand

Accepted Manuscript

Solvothermal recrystallization of α-calcium sulfate hemihydrate: Batch reactor experiments and kinetic modelling

Macedo Portela da Silva Nayane, Rong Yi, Espitalier Fabienne, Baillon Fabien, Gaunand Alain

ISSN 0022-0248

JOURNAL OF **CRYSTAL GROWTH**

Available online at www.sciencedirect.com
ScienceDirect

Solvothermal recrystallization of α-calcium sulfate hemihydrate: batch reactor experiments and kinetic modelling

Macedo Portela da Silva Nayane[a,b], Rong Yi[a,b], Espitalier Fabienne[a*],

Baillon Fabien[a], Gaunand Alain[b*]

[a] Toulouse University, Mines Albi, CNRS, RAPSODEE Center,

Campus Jarlard, F-81013 Albi CT Cedex 09, France.

[b] Paris Sciences et Lettres, Mines Paris-Tech, Center of Thermodynamics of Processes,

35 rue Saint Honoré, F-77305, Fontainebleau Cedex, France.

*corresponding author

1. Introduction

α and β-calcium sulfate hemihydrates ($CaSO_4$, ½ H_2O),are used for various applications in construction and medicine. In recent years, α sulfate hemihydrate (further noted HH), commonly known as "plaster of Paris", has been used in orthopaedics and dentistry to fill bone defects because of its excellent biocompatibility, resorption and bone repair [1, 2]. It is also widely applied in modern construction and ceramics industry, molding, special binder systems, due to its superior workability and higher strength [3, 4]. α-

calcium sulfate hemihydrate can be produced by dehydration process of natural gypsum, mainly composed of calcium sulfate dihydrate ($CaSO_4$, $2H_2O$, further noted G), dispersed in a hot aqueous phase.

Previous studies on this "water-aided" dehydration process of G into HH suggest that it occurs via a "solvothermal recrystallization" or SR route, i.e. the dissolution- of former particles and crystallization of HH [4 - 6].

The temperature ranges specified by authors depends on the conditions of synthesis. Higher temperatures (~140 °C) are applied for autoclave conditions [4]. With the use of salts, the dehydration takes place under lower temperatures. For example, temperature range of 90 – 97 °C was studied for aqueous solutions of phosphoric and sulphuric acids [7]. The transformation of G into HH in salt solution of NaCl was carried out at 85 °C [8]. The crystals of HH grow in $CaCl_2$ solutions at a fixed temperature of 90 °C [6].

Combe and Smith [4] added sodium succinate as a crystal growth modifier, crystals of HH of larger size than those of the gypsum source were therefore obtained. The addition of sodium succinate indicates that crystals of HH appeared and grew from solution, rather than from a solid-state reaction. By means of electron microscopy, Sirota et al. [8] with an aqueous solution of H_3PO_4 and H_2SO_4, as well as Yang et al. [6] in $CaCl_2$ solutions, observed the dissolution of the G crystals and formation of HH crystals within the solution. This approach was used in favor of the SR mechanism. Imahashi and Miyoshi [9] used a 5 wt% sodium chloride solution to conform the SR route from XRD patterns of the suspension and titration of the strontium ions released by the gypsum particles. FGD gypsum (Flue-Gas-Desulfurization gypsum) and a hot Ca-Mg-K chloride solution were applied at atmospheric pressure by Xiaoqin et al. [9]. They

2

suggested that the transformation of FGD into HH was monotropic, and driven by the difference in solubility between G and HH; they assumed a two stages conversion:

(1) Dissolution of G and formation of a supersaturated solution with respect to HH.

(2) Nucleation and growth of HH crystals.

They demonstrated that the size distribution and the morphology of HH crystal particles could be adjusted by altering the operating conditions, these alterations were also related to experimental growth and nucleation rates. Amin and Larson [10] conducted a kinetic study of HH crystallization from phosphoric acid solutions. They introduced population balances, considering homogeneous nucleation and growth, and determined the kinetic parameters of their rate expressions to fit the experimental size distributions. Gioia et al. [11] described a model for continuous crystallization of HH based on Amin and Larson [10] data. An homogeneous nucleation kinetic rate with an order of 2.6 was detected as well as a growth kinetic rate of first order with respect to HH supersaturation.

Nucleation and growth rates were calculated from the population number densities, using the model developed by El Moussaouiti et al. [12]. They achieved batch kinetic experiments of HH crystallization at 90°C with excess H_2SO_4 solutions and solved the population balance with the moment analysis method. They obtained a very good fit of their results considering agglomeration in addition of homogeneous and secondary nucleations and growth. Nucleation and growth rates were found of second order with respect to supersaturation.

Tang et al. [13] reported for the first time a kinetic model of HH hydrothermal production process by FGD gypsum in a batch reactor under isothermal conditions, the population balance was applied to the crystallization of HH. A non-linear optimization

3

algorithm method was used to determine the kinetic parameters of both homogeneous and secondary nucleation and growth rates, chosen as empirical power laws.

None of the studies referred to above tackles the coupling and modelling of gypsum dissolution kinetics and of HH crystallization. The purpose of this work is to undertake experiments of solvothermal recrystallization of HH in a pressurized batch stirred reactor, measure their kinetics, set up and solve a kinetic model, this will allow the testing of various assumptions on the processes involved and their rate expressions. The experiments presented here focus on the influence of the initial liquid-solid mass ratio.

2. Material and Methods

2.1 Materials

Natural gypsum from a French quarry has been used. Its chemical composition is presented in Table 1. The impurity content is around 4.2 wt%, 2.6 of which is calcium carbonate (determined by thermal gravimetry analysis coupled to mass spectrometry).

2-Propanol (C_3H_8O) was purchased from VWR France (grade 100%).

2.2 Methods

The gypsum is dispersed in an aqueous solution with different mass ratios water/solid at low temperature (R=1, 2 and 3 kg water/kg solid) and the mixture raised at 140 °C under autogenous pressure of about 4 bars. For that purpose, the mixture is set in a reactor with a working volume of 2 L (diameter of 12 cm). The agitation mobile is a three-bladed propeller of *Mixel TT* type with a diameter of 8 cm. Stirring is maintained at a speed of 500 rpm during the entire operation. The reactor is also equipped with four baffles fixed to the walls, to avoid the formation of vortex. The initial volume of solid-

4

liquid mixture is 0.9 L. Its temperature is measured by a Pt100 probe with an uncertainty of 0.1 °C during the entire trial, and the autogeneous pressure is measured by a sensor (pressure sensor BAUMER / 0-10 bars / precision 0.1 bar). The increase and stabilization of temperature at the nominal value of 140 °C are carried out using a thermostatic bath (Lauda Proline RP 845). The increase rate of temperature is about 1.65 °C/min.

2.3 Titration and granulometry

The suspension is sampled at regular time intervals to characterize the solid phase. The volume of each sample, of approximately 30 mL, is diluted in isopropanol in order to stop dissolution and crystallization.

The mass distribution of particles according to size classes is measured on the diluted samples by laser diffraction (Malvern Mastersizer 3000, range 0.01 to 3500 μm), after dilution in 2-propanol. The volume average diameter d_{43} and surface average diameter d_{32} are known within 1 μm.

To analyze the water associated in hydrated solids $CaSO_4, 2H_2O$ and $CaSO_4, 1/2H_2O$, the collected suspensions are filtered, and the powder is dried in an oven (Heraus Instruments) at 40 °C for at least 24 hours. Its water mass fraction y_W is then measured by evaporation using an infrared dryer (Ohaus MB35), where the samples are heated in a few minutes from ambient to 160 °C, then maintained at this temperature for one hour after the water release. If the gypsum used is pure, this water mass fraction $y_W(t)$ permits to estimate the mass fraction of HH, w_{HH}, in the solid mixture gypsum/HH during the synthesis.

5

From measurements, the natural gypsum contains a uniform mass fraction of anhydrated impurities, such as silica or calcium carbonate, and the mass fraction of impurities is found to be constant during the transformation. In this case, the expression of mass fraction of HH, w_{HH}, is:

$$w_{HH,EXP}(t) = \frac{y_{w0} - y_w(t)}{y_w^{th}(G) - y_w^{th}(H)} \qquad (1)$$

$y_w^{th}(G)$ is the theoretical mass fraction of water in pure gypsum (0.209) and $y_w^{th}(H)$ the theoretical mass fraction of water in HH (0.062); y_{w0} is the actual mass fraction of water found on the natural gypsum used.

Another extreme assumption consists in considering that the anhydrated impurities, such as silica or calcium carbonate, either dissolve or yield unfiltered particles proportionally to gypsum dissolved, so that they are not detected. In this case, the mass fraction of HH is:

$$w_{HH,EXP}(t) = \frac{y_w^{th}(G)(y_{w0} - y_w(t))}{y_w(t)(y_{w0} - y_w^{th}(G)) + y_{w0}(y_w^{th}(G) - y_w^{th}(H))} \qquad (2)$$

If the initial solid was pure gypsum, one simply substitutes $y_w^{th}(G)$ to y_{w0} in expressions (1) and (2), which become identical. In this work, the experimental fraction of HH in the solid mixture was evaluated with Equation (1).

3. Model

The transformation:

$$CaSO_4, 2H_2O \rightarrow CaSO_4, \tfrac{1}{2} H_2O + 3/2\ H_2O \qquad (3)$$
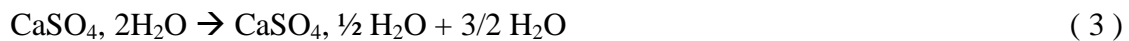
is assumed to occur according to the dissolution of hydrated solid ($CaSO_4, 2H_2O$), and crystallization of the solid ($CaSO_4, 1/2\ H_2O$):

$$CaSO_4, 2H_2O \rightarrow CaSO_4 (liq.) + 2\ H_2O \qquad (4)$$
$$CaSO_4 (liq.) + 1/2\ H_2O \rightarrow CaSO_4, \tfrac{1}{2} H_2O \qquad (5)$$

This dissolution/crystallisation mechanism, instead of a mere dehydration of particles of $CaSO_4, 2H_2O$ into particles of $CaSO_4, \frac{1}{2} H_2O$, is supported by granulometry: whilst the water content of solid sampled decreases, so does the fraction of particles of solid $CaSO_4, 2H_2O$, and a narrow peak of smaller ones appears. The respective densities of gypsum and hemihydrate are 2 305 and 2 766 kg/m^3. This weak difference between densities cannot account for the significant difference between the mean diameters of initial and final powders (see Figure 3): the particles number is not constant, which is consistent with the mechanism assumed. From the solubility data for gypsum and HH, found in the databank of the software CHESS [11] beyond a given temperature, gypsum becomes more soluble than solid HH, and the crystallization of HH makes the dissolution of gypsum possible (Figure 1). The model thereafter aims to evaluate several assumptions on the dissolution, nucleation and growth processes, the corresponding kinetic expressions, and to fit their parameters using the kinetic results obtained during batch experiments. The mass distribution of initial gypsum particles is divided into classes of size L between 0.8 and 120 µm: each class *i* contains a mass fraction given by preliminary size analysis (Figure 2). The model takes into consideration the instantaneous dissolution rate of each class. It provides the variation of the moments of the density function of crystallizing particles, via usual relations deduced from the population balance [17].

3.1 Dissolution

Let be the extent of dissolution of gypsum for particles of the size class i ($X_{G,i}$):

$$X_{G,i} = \frac{\left(m_{G,i}^0 - m_{G,i}\right)}{m_{G,i}^0} \qquad (6)$$

7

$m_{G,i}^{0}$ is the initial mass of gypsum in this class and $m_{G,i}$ is the one at time t. $X_{G,i} = 1$ at complete dissolution.

Its instantaneous increase is related to the flux J_{Di} (mol.m^{-2}.s^{-1}) of solute leaving the surface of particles of class i. If one assumes that the volume of a particle is proportional to its mass, this surface is proportional to $(1- X_{G,i})^{2/3}$, then:

$$\frac{dX_{G,i}}{dt} = K_{0,i} \left(1 - X_{G,i}\right)^{2/3} J_D \qquad (7)$$

where $K_{0,i} = \dfrac{1}{L_{G,i}(t=0)} \dfrac{\phi_{S,G}}{\phi_{V,G}} \dfrac{M_G}{\rho_G}$; M_G (kg/mol) is the molar mass of gypsum; $\phi_{S,G}$ and $\phi_{V,G}$ are the surface factors and volume factors of gypsum particles; $L_{G,i}$ (t=0) is the initial characteristic size of gypsum particles in class i and ρ_G (kg/m^3) is the density of gypsum particles. The surface and volume factors of gypsum particles are assumed independent of particle size.

Dissolution kinetics are frequently controlled by mass transfer to the solution. We made this assumption for a first use of the model, then:

$$J_D = k_{L,i}^{G} \rho_w \left(C_{G,eq} - C_G\right) \qquad (8)$$

where $C_{G,eq}$ (mol/kg water) is the concentration of gypsum at equilibrium (given in Figure 1); C_G (mol/kg water) is the bulk concentration of gypsum at time t and ρ_w is the density of water, function of temperature.

The transfer coefficient $k_{L,i}^{G}$ (m/s) is given by the correlation from Armenante and Kirwan [12]:

$$Sh = \frac{k_{L,i}^{G} L_i}{D} = 2 + 0,52 \left(\frac{L_i^{4/3} \varepsilon_m^{1/2}}{\nu}\right)^{0,52} \left(\frac{\nu}{D}\right)^{1/3} \qquad (9)$$

8

D (m^2/s) is the diffusion coefficient of the solute, and v (m^2/s) is the kinematic viscosity of water. The diffusion coefficient is set to 9.1 10^{-10} m^2/s.

The mean rate of energy dissipation ε_m (W/kg) in the reactor depends on the power number of the stirrer N$_P$:

$$\varepsilon_m = \frac{N_p N^3 d_a^5}{V} \tag{10}$$

where N(s^{-1}), d$_a$ (m) and V(m^3) are respectively the stirring speed, the diameter of the stirrer and the volume of solid-liquid mixture.

For our experiments, the Reynolds number $Re = \frac{N d_a^2}{v}$ is always higher than 10^4, indicating turbulent mixing, and N$_p$ = 0.7 (data from the supplier). For initial mass ratios water/solid R of 1, 2 and 3 kg/kg, ε$_m$ is respectively 2.1, 1.4 and 1.4 W/kg (the volume of mixture is the same for the two last experiments). The fraction of the initial amount of gypsum dissolved at time t is then:

$$X_{Gm} = \frac{\sum_i m_{Gi}^0 X_{Gi}}{m_G^0} \tag{11}$$

with: $m_G^0 = \sum_i m_{Gi}^0$ (12)

3.2 Crystallisation

The instantaneous population balance of HH particles has to take into account that the mass of water m$_w$ (kg) increases gradually as the gypsum dissolves and the HH crystallizes:

$$m_w . B . \delta\left(l - l^*\right) = \frac{\partial}{\partial t}\left(n_{HH}(l).m_w\right) + m_w \frac{\partial}{\partial l}\left(G.n_{HH}(l)\right) \tag{13}$$

9

where $n_{HH}(l)$ dl represents the number of HH particles per unit mass of water contained in the size class [l ; l + dl[; B (nber/(kg.s)) is the nucleation rate; G (m/s) is the growth rate, and l^* (m) is the size of nuclei (m). $\delta(l-l^*)$ is the Dirac function, and is equal to 1 for $l=l^*$ else it is 0.

Assuming that the growth rate G of a HH particle is independent of its size (Mac Cabe assumption), simple relations between the moments $\mu_j = \int_0^\infty n_{HH}(l) l^j \, dl$ (m^j/kg water) of the density function n_{HH} are found based on the previous population balance:

$$\frac{\partial}{\partial t}\left(m_w . \mu_j\right) = j.G.\mu_{j-1} \, m_w + 1^{*j}.B.m_w \qquad (14)$$

This method is also available for a population with weak size dispersion, if one estimates G for its mean size μ_3/μ_2. Disregarding the contribution of nuclei in the population of particles, which is often the case in crystallization, leads to the following relations concerning the five first moments:

$$\frac{d}{dt}\left(\mu_0\right) = B - \frac{\mu_0}{m_w}\frac{d}{dt}\left(m_w\right) \qquad (15)$$

$$\frac{d}{dt}\left(\mu_j\right) = j.G.\mu_{j-1} - \frac{\mu_j}{m_w}\frac{d}{dt}\left(m_w\right) \qquad (16)$$

where j = 1 to 4.

The nucleation rate B as well as the growth rate G depend on the super-saturation ratio S with respect to the HH solubility $S=\dfrac{C_{CaSO_4}}{C_{HH,eq}}$, where $C_{HH,eq}$ (mol/kg water) is the saturation concentration of $CaSO_4$, that would be at equilibrium with HH at temperature

10

T, (from solubility data used in Figure 1), and C_{CaSO_4} (mol/kg water) is the concentration of $CaSO_4$ in solution, derived from the conservation equation (21). Two processes contribute to nucleation: primary nucleation – homogeneous or heterogeneous, if at the surface of gypsum particles - is compulsory in an unseeded batch reactor, and we choose the usual kinetic expression [17]:

$$B_1 = k_{n1} \exp\left(-\frac{4}{27} \frac{\phi_{S,G}^3}{\phi_{V,G}^2} \frac{\gamma^3 v_0^2}{\left(k_B T\right)^3 \ln(S)^2} \right) \tag{17}$$

Once a sufficient mass of HH particles is formed, especially in crystallization processes, secondary nucleation may prevail, and we introduce the usual kinetic expression:

$$B_2 = k_{n2} \left(S-1\right) \mu_3^{n2} \tag{18}$$

where γ (J/m^2) is the surface tension crystal/solution; v_0 (m^3/molecule) is the molecular volume of HH in a solid form; k_B (J/(molecule.K)) is the Boltzmann number; k_{n1} (nber/(kg water.s)) and k_{n2} ($m^{-3.n2}$/s/kg water^{n2-1}) are the kinetic constants of the two nucleation rates. The total rate B is then the sum B_1+B_2. The usual expression of growth rate is introduced:

$$G = k_g \left(S-1\right)^g \tag{19}$$

The variation of the instantaneous mass of water is found from its conservation equation:

$$m_W = m_W^0 - \left(1 - \frac{M_{CaSO_4}}{M_G}\right) m_G^0 \left(1 - X_{Gm}\right) - \left(1 - \frac{M_{CaSO_4}}{M_{HH}}\right) \varphi_{V,HH} \rho_{HH} \mu_3 m_w \tag{20}$$

where M_{CaSO_4} is the molar mass of anhydrous solid (kg/mol), $\varphi_{V,HH}$ and ρ_{HH} (kg/m^3) are respectively the volume factor (assumed independent of particle size) and the density of HH particles. The variation of the instantaneous concentration of solute is

11

also found from a mass balance, which relates it to the extent of dissolution of gypsum and to the amount of HH crystallized:

$$C_{CaSO_4} = \frac{\dfrac{m_G^0 X_{Gm}}{m_W} - \phi_{V,HH} \rho_{HH} \mu_3}{M_{CaSO_4}} \qquad (21)$$

The mass variation for water saturation of the gas phase can be disregarded.

4. Results and discussion

4.1 Experimental Results

Figure 3 shows the variation of the average sizes d_{43} and d_{32}, found from the mass size distributions of samples, and Figure 4 the increase of the mass fraction of HH $w_{HH,EXP}(t)$ in the powder samples. In these figures, time 0 is when the temperature in the reactor reaches 120 °C, before reaching the set value of 140 °C.

For the conditions investigated, the transformation takes place within 10 minutes; the water/solid ratio R and the mean rate of energy dissipation ε_m have little influence on the variation of $X_{HHm,exp}$ and of the two average sizes. The significant decrease of these diameters is in agreement with a dissolution-recrystallization of HH, instead of a mere solid-solid transformation of gypsum particles. However, the mass fraction of HH, as calculated from relation (1), stabilizes at values lower than 1, which shows that the gypsum used contains impurities. Using purified gypsum leads to a final mass fraction of HH equal to 0.98, the difference to 1 is within the experimental error from the water content measurement.

The surface of solid impurities of gypsum, if insoluble, may be used for heterogeneous nucleation; they may also change the speciation of the solution if they dissolve.

4.2 Solution of the model and kinetic identification

The system of ordinary differential equations was solved with the software MATLAB, using the ode15s (variable stiff solver). For a first step, gypsum and HH particles observed by microscope, are considered as spherical. The volume factor ($\phi_{V,k}$, k=G or HH) and the surface factor ($\phi_{S,k}$, k=G or HH) are then respectively equal to $\pi/6$ and π. The experimental values are compared to those given by the model, respectively $w_{HH,CAL}$ and mean diameters $d_{43,CAL}$ and $d_{32,CAL}$:

$$w_{HH,CAL} = \frac{\phi_{V,HH}\rho_{HH}\mu_3}{\phi_{V,HH}\rho_{HH}\mu_3 + m_G^0\left(1-X_{Gm}\right)} \tag{22}$$

$$d_{43,CAL} = \frac{\sum\limits_{i=1}\dfrac{m_{Gi}^0 L_{i0}(1-X_{Gi})^{4/3}}{\rho_G} + m_w\phi_{V,HH}\mu_4}{\sum\limits_{i=1}\dfrac{m_{Gi}^0(1-X_{Gi})}{\rho_G} + m_w\phi_{V,HH}\mu_3} \tag{23}$$

$$d_{32,CAL} = \frac{\sum\limits_{i=1}\dfrac{\phi_{S,G}}{\phi_{V,G}\rho_G} m_{Gi}^0 (1-X_{Gi}) + m_w\phi_{S,HH}\mu_3}{\sum\limits_{i=1}\dfrac{\phi_{S,G}}{\phi_{V,G}\rho_G}\dfrac{m_{Gi}^0}{L_{i0}}(1-X_{Gi})^{2/3} + m_w\phi_{S,HH}\mu_2} \tag{24}$$

The kinetic constants and orders of reaction k_{n1}, k_{n2}, k_g, $b2$, $n2$, g, and the interfacial tension γ between crystal of HH/solution, are fitted to given values to minimize an objective function f_{min} on $w_{HH,CAL}$, $d_{43,CAL}$ and $d_{32,CAL}$ for the three experiments:

13

$$f_{min} = \sum_t \sum_{i=1}^{3} \left(w_{HH,i,CAL}(t) - w_{HH,i,exp}(t) \right)^2 + \sum_t \sum_{i=1}^{3} \left(\frac{d_{43,i,CAL}(t) - d_{43,i,exp}(t)}{d_{43,i,exp}(t)} \right)^2 + \dots$$
$$\sum_t \sum_{i=1}^{3} \left(\frac{d_{32,i,CAL}(t) - d_{32,i,exp}(t)}{d_{32,i,exp}(t)} \right)^2 \tag{25}$$

The fitted parameters are given in Table 2. The continuous curves in Figures 3 to 8 have been calculated with these parameters.

The mean sizes and their final values are properly represented. The peaks of both experimental and calculated average sizes at the time of transformation (about 18 min) correspond to the disappearance of finest particles of gypsum, just before particles of HH nucleate and grow.

Figure 5 shows the evolution of the extent of dissolution of gypsum for particles of different initial size. The first plateau observed for all sizes shows that the solution is very quickly at equilibrium with gypsum, compared to the rate of temperature increase. When gypsum becomes more soluble than HH – when the temperature approximately reaches 108 °C, the extent of dissolution increases drastically for all particle sizes, with a slower rate for particles of higher initial size. HH Nucleation and growth rates are shown in Figures 6 and 7. The calculated growth rate does not actually correspond to a growth of particles of HH as long as HH does not nucleate. For a better understanding, the primary nucleation rate is plotted on a small range (between 7 and 10 min), and the secondary nucleation rate during all the transformation. The primary nucleation triggers the production of first, crystals, growing thanks to the supersaturation of the solution (Figure 8). Within a few minutes, secondary nucleation, triggered by the production of HH crystals and less sensitive to the supersaturation replaces primary nucleation (Figure 6).

14

Especially, when the initial water/solid mass ratio R decreases, the experimental final average size decreases, which is corroborated by the model: the rate of secondary nucleation is slightly higher, which must lead to more particles of lower final sizes, and the growth rate decreases faster (Figures 5 and 6).

An interfacial tension of 0.092 J/m^2 has been estimated at 140 °C from the following correlation [17]:

$$\gamma_{HOM} = k_B T K \left(N_A C_C\right)^{2/3} ln\left(\frac{C_C}{C'_{HH,eq}}\right)$$

(26)

with $C_c = \rho_{HH}/M_{HH}$ the molar density of HH, [mol/m^3] ; $C'_{HH,eq}$ the saturation concentration of HH [mol/m^3], at temperature T [K], N_A the Avogadro number [molecules/mol] and K = 0.414 a geometrical factor. The fitted interfacial tension γ is about 4 times lower than this value, which suggests that the primary nucleation could be heterogeneous, at the surface of gypsum particles or on solid impurities produced at the beginning of their dissolution.

In order to explain the two peaks of supersaturation found from the model between 5 and 15 minures (Figure 8), the temperature, the equilibrium molal concentrations of Ca, $C_{HH,eq}$ and $C_{G,eq}$ and its concentration in the solution, [Ca], are reported and compared for a mass ratio water/solid R=1 (Figure 9). During this period, the temperature of the suspension increases then reaches 140 °C.

From the evolution of Ca, we can identify four steps in the dissolution-recrystallization process.

In the first one (I), [Ca] remains constant, although the temperature increase leads to lower solubility of both gypsum G and hemihydrate HH, then the supersaturation ratio

15

S_{HH} with respect to HH increases: this comes from a slow dissolution kinetics of gypsum. Nine minutes after, HH begins to crystallize: its nucleation (Figure 6), then (mainly) growth (Figure 7) consume the Ca species, its concentration gets back to gypsum solubility $C_{G,eq}$, and S_{HH} decreases (step II). Between 9.7 and 11.7 min (step III), [Ca] equals $C_{G,eq}$: the crystallization of HH is the limiting step of the transformation; as $C_{G,eq}$ decreases more rapidly with T than $C_{HH,eq}$, S_{HH}, which is now equal to the ratio $C_{G,eq}/C_{HH,eq}$, increases. After 11.7 min (step IV), the temperature is constant and equal to 140 °C, the crystallization of HH goes on and consumes the Ca in solution; now, dissolution doesn't manage to compensate the consumption of Ca, so that [Ca] and S_{HH} decrease.

5. Conclusion

In this work, a new experimental device suitable for kinetic studies of solid-liquid reactions and crystallizations beyond the boiling point of water at atmospheric pressure has been developed. A partially dehydrated solid ($CaSO_4$, $1/2H_2O$) is obtained from a solid hydrated natural product ($CaSO_4$, $2 H_2O$) dispersed in the aqueous phase at different water/solid ratios under autogenous pressure of about 4 bars.

The apparatus is equipped with a sampling device, which allows to characterize the kinetics thanks to size distribution and water content measurements on the solid phase of samples. We developed, and solved via a MATLAB routine, a model considering the dissolution of the initial particles of gypsum, and the crystallization of the solid calcium hemihydrate, via primary and secondary nucleation and growth. It takes into account the dissolution of each class of this distribution separately, and provides the moments of the population of particles of hemihydrate, based on their population balance. Different mechanisms of dissolution and crystallization can be assessed. From now on, we

16

assumed that dissolution was controlled by transfer. A satisfying representation of kinetic results has been obtained – namely the variations with time of the extent of the transformation and of the two average sizes d_{43} and d_{32}. For this representation, secondary nucleation had to be considered together with primary nucleation, which is consistent with the low supersaturation ratio arising during the transformation. The final hemihydrate mass fractions found from water titration are lower than one, which suggests that the gypsum contains impurities, which has not yet been taken into account by the model.

Acknowledgment

References

[1] Fan L.; Jianli L.; Guangyong Y.; Zongyou P.; Xiao N.; Huazi X.; Qing H.; Effect of pH and succinic acid on the morphology of α-calcium sulfate hemihydrate synthesized by a salt solution method. *J of Cryst Growth*, vol. 374, pp. 31–36, 2013.

[2] Jianmin C.; Jun G.; Hengbo Y.; Fanggang L.; Wang A.; Yongqiang Z.; Zhanao W.; Tingshun J.; Daming Q.; Bujun C.; Yuqin J.; Min S. Size-controlled preparation of α-calcium sulphate hemihydrate starting from calcium sulphate dihydrate in the presence of modifiers and the dissolution rate in simulated body fluid. *Mat Sci and Eng*. vol. 33, 3256–3262, 2013.

[3] Ling Y.; Demopoulos G. Preparation of alpha-Calcium Sulfate Hemihydrate by Reaction of Sulfuric Acid with Lime. *Ind. Eng. Chem. Res.*, vol 44, pp. 715-724, 2005

[4] Combe and Smith, Studies on the preparation of calcium sulphate hemihydrate by an autoclave process, *J. appl. Chem.,* vol. 18, 307-312, 1968.

[5] Zurz A. ; Odler I. ; Thiemann F. ; Berghofer K. Autoclave-Free Formation of α-Hemihydrate Gypsum, *J. Am. Ceram. Soc.*, vol 74, 1117-1124, 1991.

[6] Yang L. ; Wu Z. ; Guan B. ; Fu H. ; Ye Q. Growth rate of a-calcium sulfate hemihydrate in K–Ca–Mg–Cl–H2O systems at elevated temperature, *Journal of Crystal Growth*, vol. 311, pp. 4518–4524, 2009.

[7] Sirota I. S.; Dorozhkin S. V.; Kruchinina M. V. ;Melikhov I. V. ; Phase transformation and dehydration of calcium sulphate dihydrate in solution studied by SEM. *Scanning,* vol. 14, pp. 269–275, 1992.

[8] Imahashi M. and Miyoshi. T. Transformations of gypsum to calcium-sulfate hemi-hydrate and hemihydrate to gypsum in NaCl solutions. Bulletin of the Chemical Society of Japan, vol. 67, pp. 1961–1964, 1994.

[9] Xiaoqin W.; Shitang O.; Baohong G.; Zhongbiao W. Transformation of Flue-Gas-Desulfurization Gypsum to Hemihydrated Gypsum in Salt Solution at Atmospheric Pressure. *Chin. J. Polym. Sci*., vol. 19(2), 349 – 355, 2011.

[10] Amin A.B. and M.A. Larson M.A., Crystallization of calcium sulfate from phosphoric acid, *Ind. Eng. Chem. Proc. D. D*., vol. 7(1), 133-137, 1968.

[11] Gioia F.; Mura G.; Viola A. Analysis, simulation, and optimisation of the hemihydrate process for the production of phosphoric acid from calcareous phosphorites, *Ind. Eng. Chem. Proc*., vol. 16, pp. 390-399, 1977.

[12] Moussaouiti M.; Boistelle R.; A. Bouhaouss, Klein P. Crystallization of calcium sulphate hemihydrate in concentrated phosphoric acid solutions. *Chem. Eng. J*., vol. 68, pp. 123-330, 1997

[13] Tang M.; Li X.; Shen Y.; Shen X. Kinetic model for calcium sulfate [alpha]-hemihydrate produced hydrothermally from gypsum formed by flue gas desulfurization *J. Appl. Cryst*. vol. 48, pp. 827-835, 2015.

[14] Van der Lee, J. Thermodynamic and mathematical concepts of CHESS. Technical Report LHM/RD/98/39, CIG, Ecole des Mines de Paris, Fontainebleau, France, p. 99. 1999.

[15] Armenante, P.M. and Kirwan, D.J. Mass transfer to microparticles in agitated systems, *Chem. Eng. Sci*. vol. 44, pp. 2781-2796, 1999.

[16] O. Sohnel, J. Garside. Precipitation: Basic Principles and Industrial Applications. BUTTERWORTH-HEINEMANN, 1992

[17] A. Mersmann, Crystallization technology handbook, Marcel Dekker, 2nd edition, 2001, chapter 1, New York , Marcel Dekker

List of figures

Figure 1. Calculated solubilities of calcium sulphate dihydrate and calcium sulphate hemihydrate as function of temperature

Figure 2. Mass distribution of initial gypsum particles

Figure 3. Evolution of the average sizes d_{43} and d_{32} of these powders for different initial mass ratios water/gypsum. The continuous curves were calculated from the model with the parameters given in table 2. The experimental points were evaluated from mass distribution of particles according to size classes determined by laser granulometry.

Figure 4. Evolution of the fraction of hemihydrate transformed in powders sampled for different initial mass ratios water/solid gypsum. The continuous curves were calculated from the model with the parameters given in table 2. The experimental points were evaluated with equation (1).

Figure 5. Conversion rates of gypsum particles as function of their size calculated from the model with the parameters given in table 2. Top to down the size of particles increases.

Figure 6. Primary nucleation and secondary nucleation rates for different initial mass ratios water/gypse calculated from the model with the parameters given in table 2.: (a) Primary nucleation rate (b) Secondary nucleation rate.

Figure 7. Growth rate during the synthesis for different initial mass ratios water/gypsum calculated from the model with the parameters given in table 2.

20

Figure 8. (a) Supersaturation ratio during the synthesis for different initial mass ratios water/gypsum calculated from the model with the parameters given in table 2.

(b) zoom of the second peak.

Figure 9: Evolution of calcium concentration [Ca], temperature and saturation concentrations, CHH,eq and CG,eq expressed in Ca molal concentrations. Mass ratio water/solid R=1
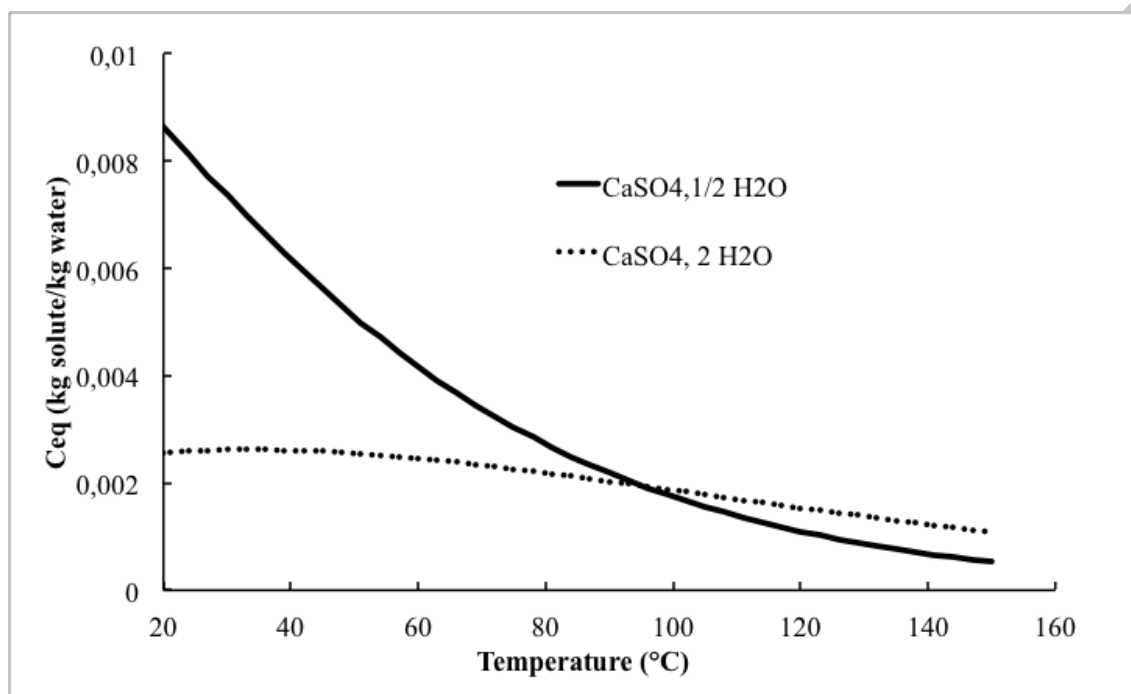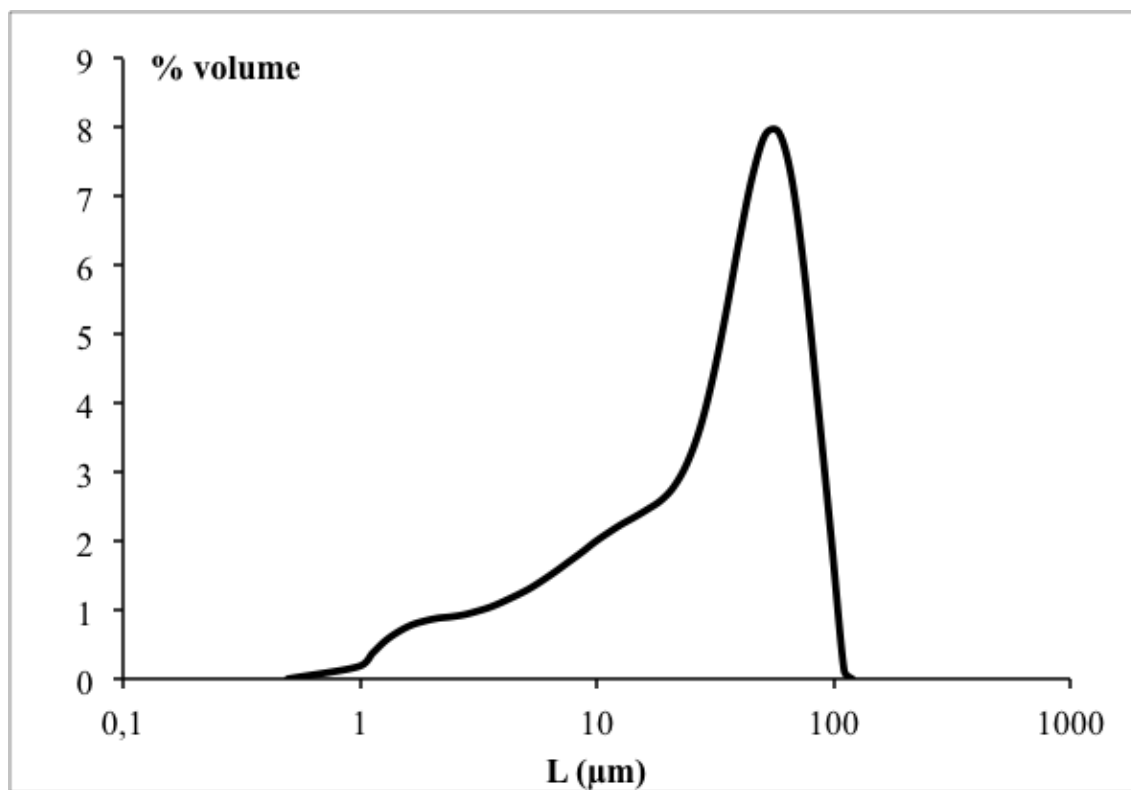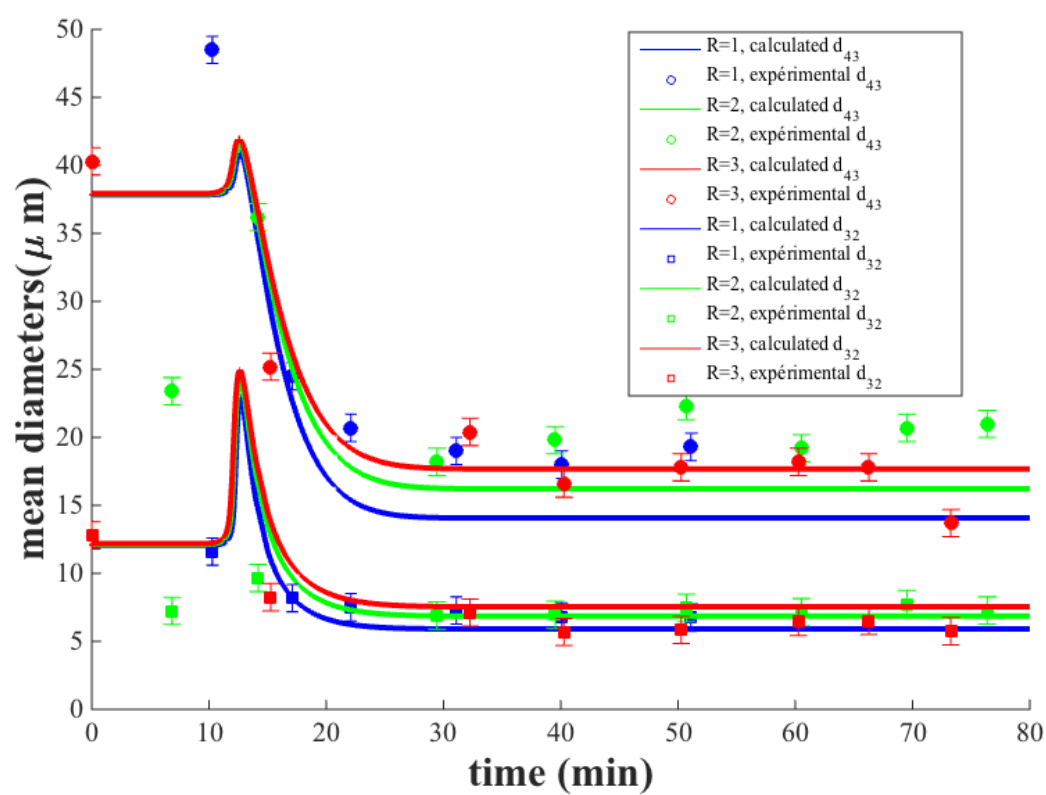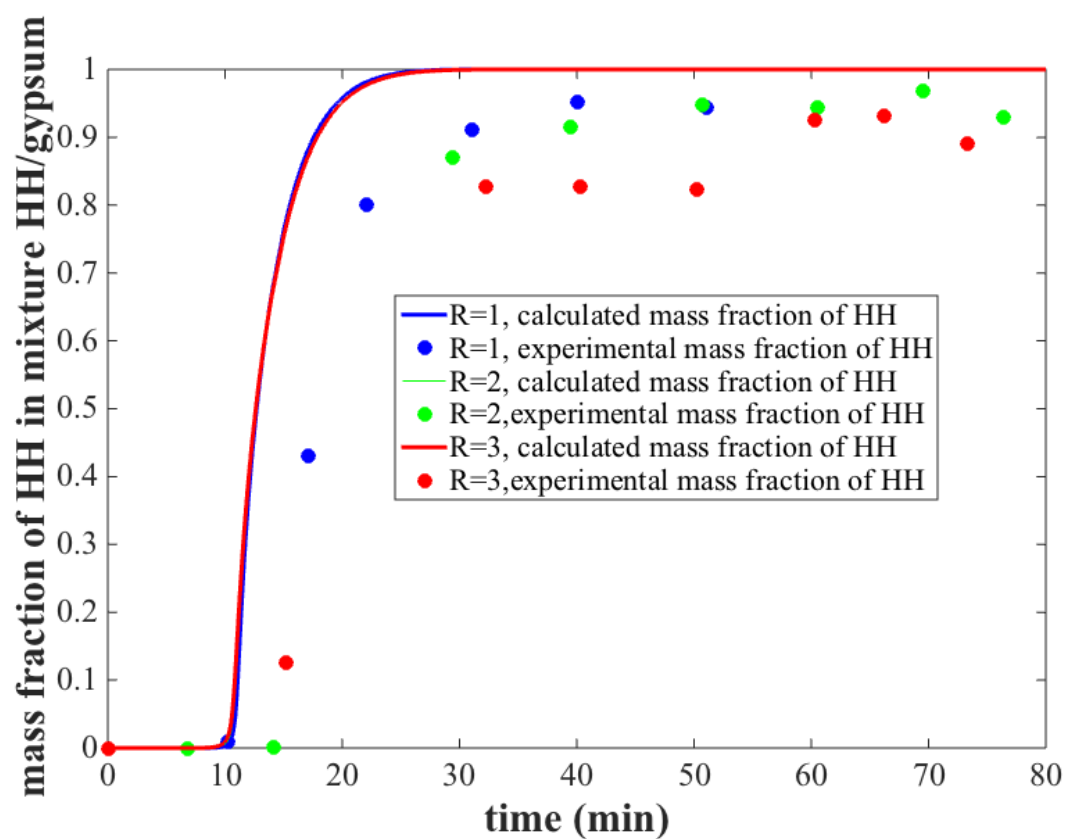
Figure 1

Figure 2

Figure 3

Figure 4

Figure 5
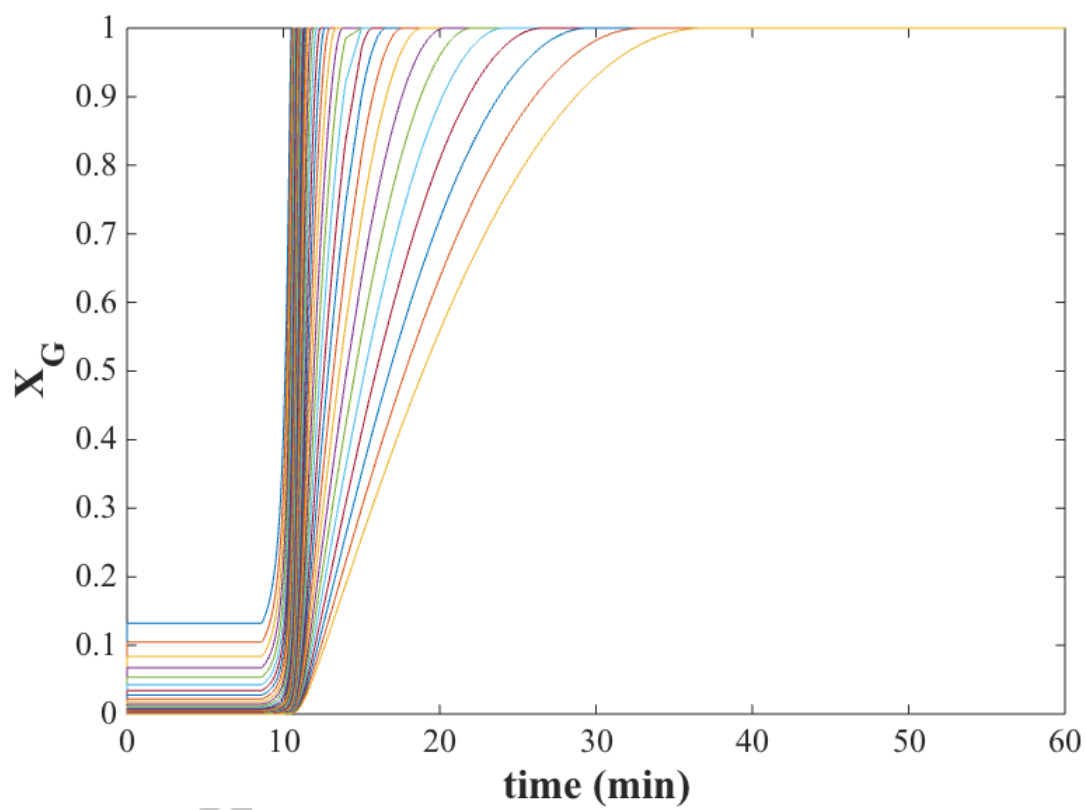
Figure 6
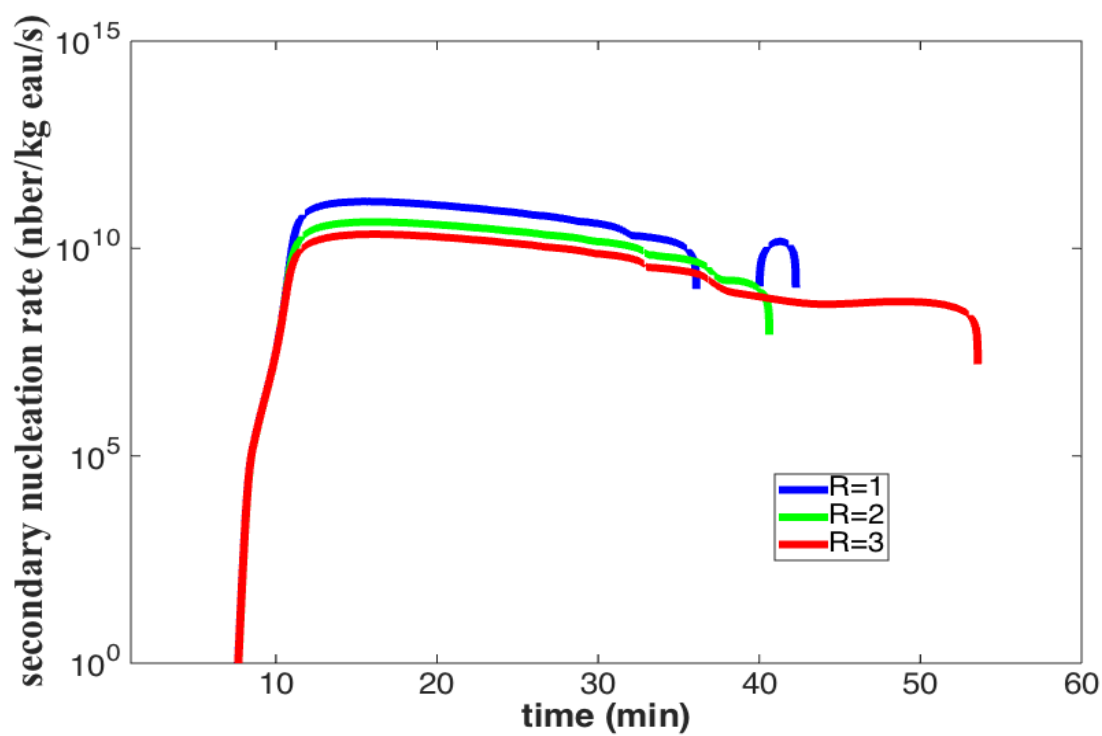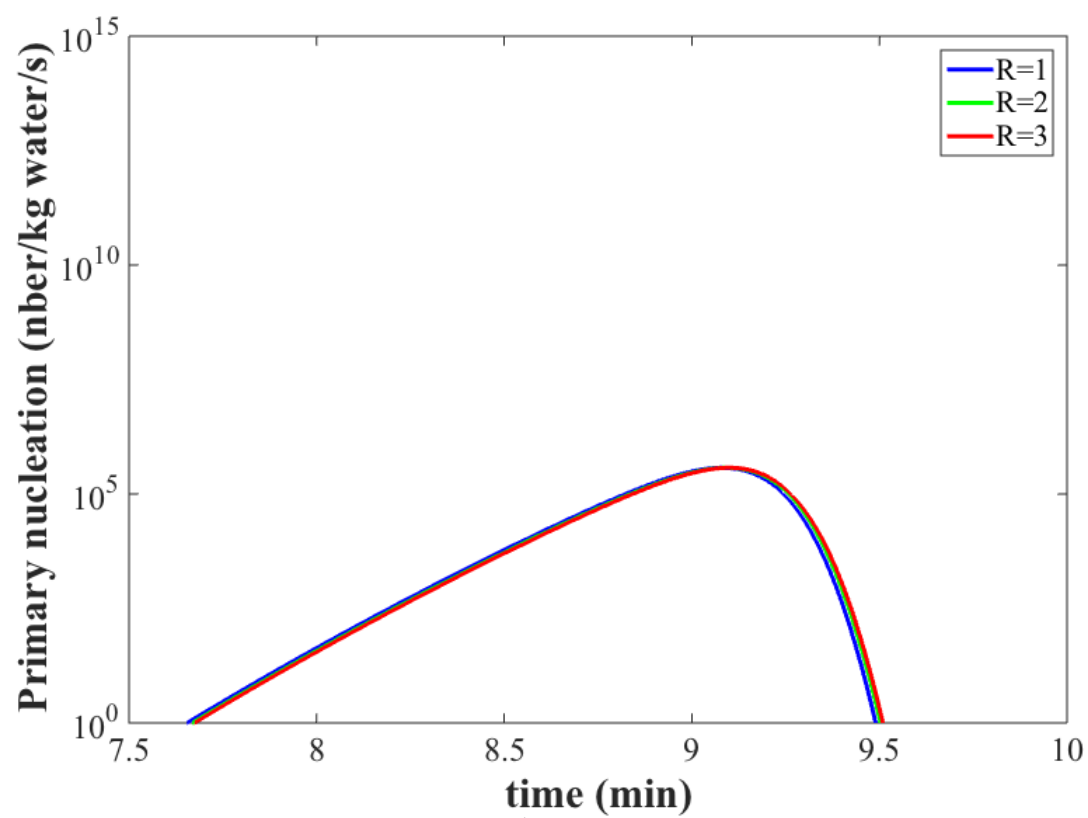
Figure 7
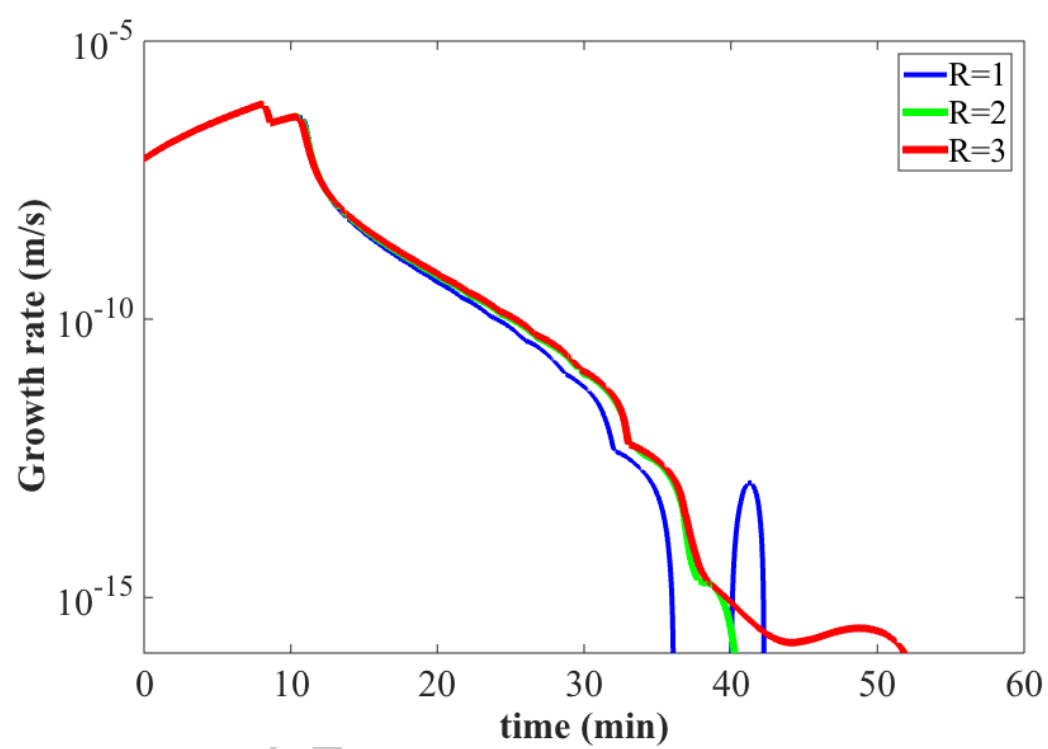
Figure 8
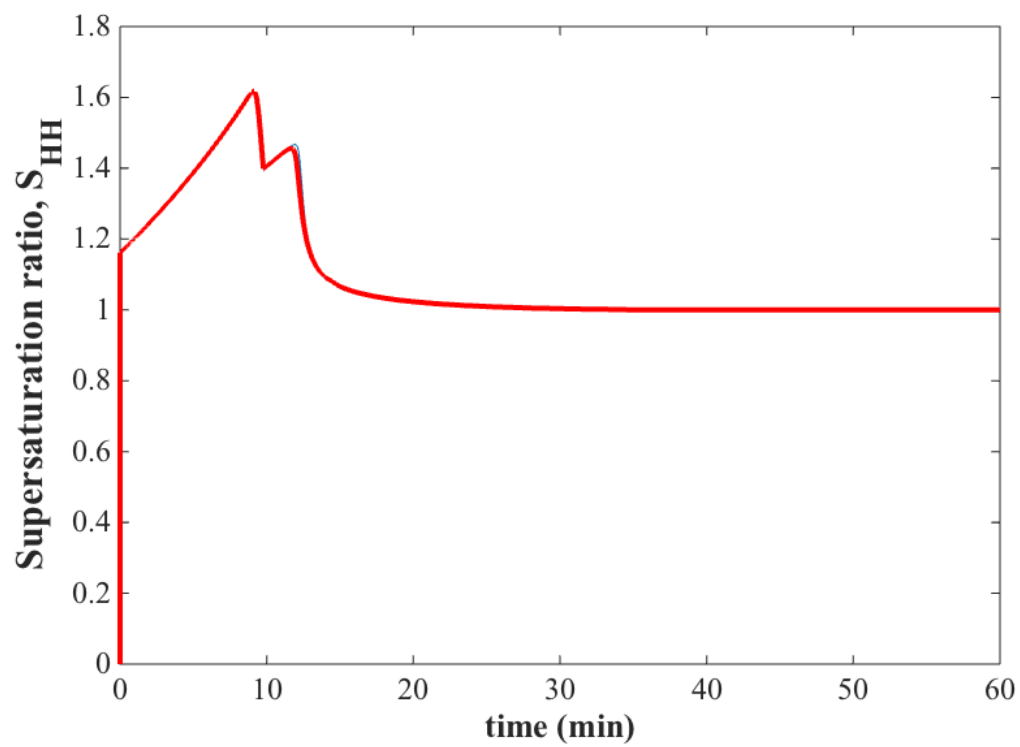
(a)
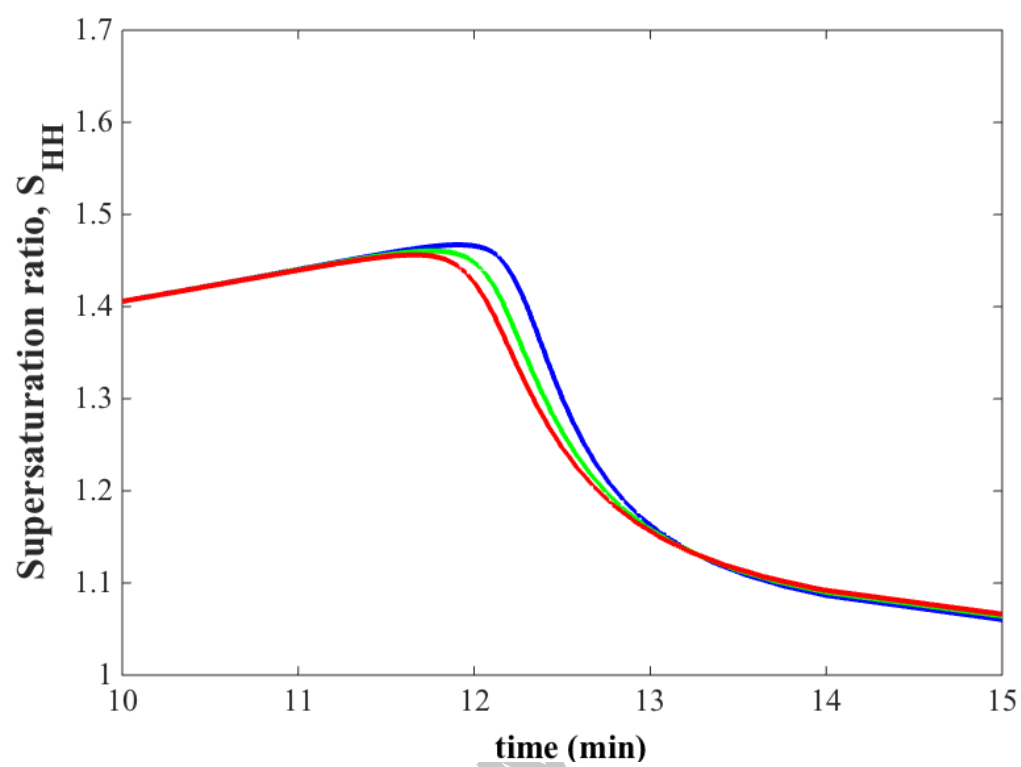
(b)

Figure 9
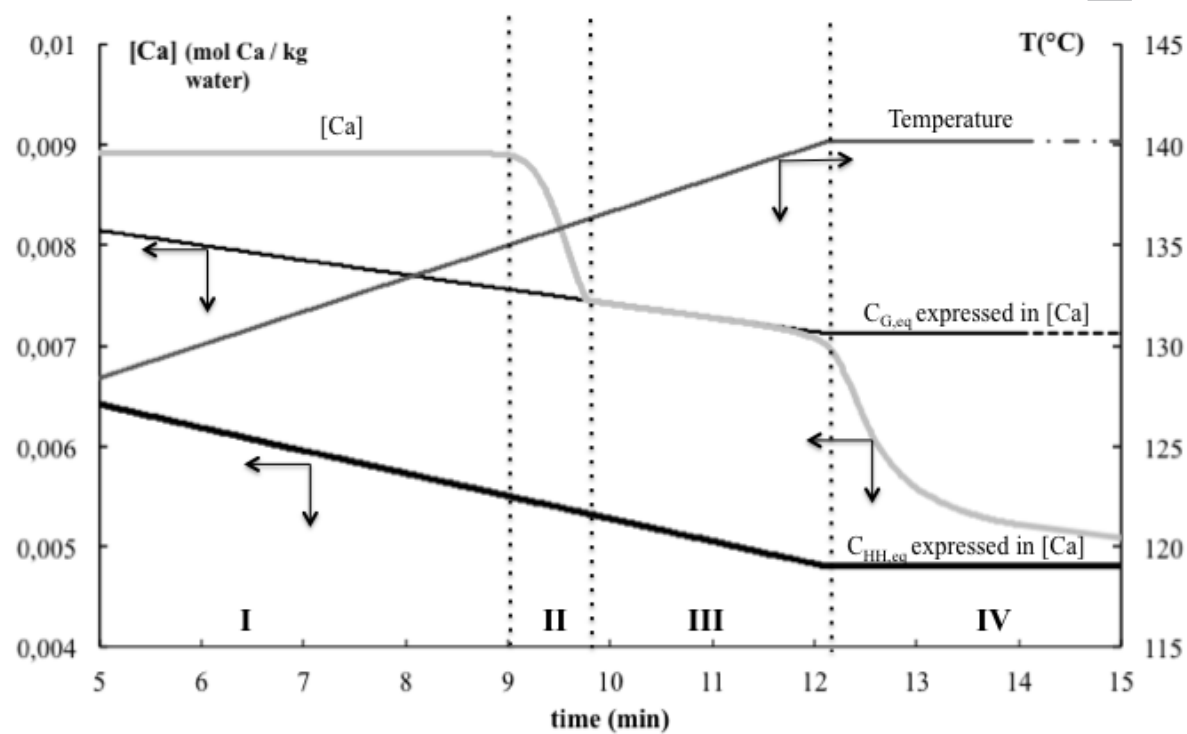
List of Tables

Table 1

Constituents	Wt %
MgO	1.54
Al_2O_3	0.47
SiO_2	1.77
SO_3	40.01
K_2O	0.03
CaO	35.25
Fe_2O_3	0.10
SrO	0.26

	Primary nucleation		Secondary nucleation			Growth	
	$k_{n1}(*)$ $(1/(kg.s))$	$\gamma(*)$ (J/m^2)	$k_{n2}(*)$ $(m^{-3n2}/s/kg^{n2})$	n2	b2(*)	$k_g(*)$ (m/s)	g
Identified values	$2.98\ 10^{25}$	0.0246	$5.19\ 10^{11}$	0.5	1.81	$1.91\ 10^{-6}$	2

Objective function: f_{min}/N_{points} = 0.050; Npoints: number of measured data